

PAPER • OPEN ACCESS

Photo-induced viscoelasticity in cytocompatible hydrogel substrates

To cite this article: Ian A Marozas *et al* 2019 *New J. Phys.* **21** 045004

View the [article online](#) for updates and enhancements.

Recent citations

- [The Plot Thickens: The Emerging Role of Matrix Viscosity in Cell Mechanotransduction](#)
Marco Cantini *et al*
- [Engineered Biomaterial Platforms to Study Fibrosis](#)
Matthew D. Davidson *et al*
- [Phototunable Viscoelasticity in Hydrogels Through Thioester Exchange](#)
Benjamin J. Carberry *et al*



PAPER

Photo-induced viscoelasticity in cytocompatible hydrogel substrates

OPEN ACCESS

RECEIVED

30 November 2018

REVISED

19 February 2019

ACCEPTED FOR PUBLICATION

25 March 2019

PUBLISHED

15 April 2019

Original content from this work may be used under the terms of the [Creative Commons Attribution 3.0 licence](https://creativecommons.org/licenses/by/4.0/).

Any further distribution of this work must maintain attribution to the author(s) and the title of the work, journal citation and DOI.

Ian A Marozas^{1,2}, Justin J Cooper-White^{3,4} and Kristi S Anseth^{1,2}¹ Department of Chemical and Biological Engineering, University of Colorado, Boulder, CO 80303, United States of America² BioFrontiers Institute, University of Colorado, Boulder, CO 80303, United States of America³ The UQ Centre in Stem Cell Ageing and Regenerative Engineering (StemCARE), Australian Institute for Bioengineering and Nanotechnology, The University of Queensland, St. Lucia, QLD 4072, Australia⁴ School of Chemical Engineering, The University of Queensland, St. Lucia, QLD 4072, AustraliaE-mail: kristi.anseth@colorado.edu**Keywords:** hydrogel, allyl sulfide, adaptable networks, viscoelasticity, mechanotransduction, AFCTSupplementary material for this article is available [online](#)**Abstract**

Human mesenchymal stem cells (hMSCs) sense and respond to the bulk elastic and viscoelastic properties of their microenvironment, as well as the spatial distribution of these mechanical signals. Hydrogel substrates with photo-controlled mechanical properties can allow one to probe the cellular response to localized variations in substrate viscoelasticity. Here, we report on a cytocompatible hydrogel culture system that allows photo-induced changes in viscoelasticity via an addition-fragmentation chain transfer reaction triggered by a network tethered photoinitiator. Tethering the photoinitiator to the network allowed for on-demand material property changes and spatiotemporal control of viscoelasticity. It was found that both the photoinitiation rate and chain transfer agent concentration contributed to the degree of photo-induced viscoelasticity. The loss factor ($\tan \delta$) of this system was tuned with the illumination intensity and chain transfer agent concentration, with a maximum value of 0.27 at 1 rad s⁻¹. In experiments with hMSCs cultured on the hydrogels, the cellular protrusions retracted in response to photo-induced viscoelasticity and this retraction could be confined to a single cellular protrusion through controlled photo-illumination. The retraction length and area of each protrusion was dependent on the initial proximity to the viscoelastic region.

1. Introduction

Many cells are anchorage-dependent and reside within the interstitial space of tissues, embedded in a protein-rich extracellular matrix (ECM). These cells are physically coupled to the ECM through integrin connections and exert a stress on it through actomyosin contractility. The resulting deformation of the ECM informs the cells about the mechanical properties of their microenvironment and can ultimately lead to a change in the production of cytoskeletal proteins and cytoskeletal stress [1, 2]. Physiologically, these biophysical signals provide cells with critical information necessary for the development, maintenance, function, and wound healing of tissues [3–5]. Thus, a better understanding of the mechanisms by which cells perceive biophysical signals that ultimately affect transcriptional regulation and cytoskeletal organization, in a process called mechanotransduction, will help inform the design of future therapeutic biomaterials for functional tissue generation.

Synthetic hydrogels have for some time been employed as cell culture substrates to probe the conversion of biophysical inputs into chemical outputs via mechanotransduction [3, 5–8]. Synthetic gels allow for systematic tuning of the properties of the matrix, but oftentimes, the final materials are covalently cross-linked, rendering them purely elastic with respect to their mechanical properties. However, there is a growing interest in the development of viscoelastic synthetic hydrogels [9, 10], as most tissue are viscoelastic in nature [11, 12]. Under an imposed load or stress, the viscous component of a viscoelastic substrate is energy dissipative and gives rise to various time-dependent phenomena including creep—a time-dependent increase in deformation (i.e. strain) under an imposed constant stress—and stress relaxation—a time-dependent decrease in stress at constant

strain. These viscoelastic processes are thought to be an important component of the biophysical signals that direct tissue specific cell function through mechanotransduction [10]. Indeed, human mesenchymal stem cells (hMSCs) cultured on high-creep hydrogels spontaneously differentiate towards a smooth muscle cell lineage and also exhibit a greater potential for multipotent differentiation compared to low-creep hydrogel [13, 14]. The concept of tissue specific mechanotransduction is also supported by the fact that the characteristic timescales of viscoelastic processes varies largely between tissues. For instance, a recent study found that bone fracture hematoma dissipate stress much faster than brain or liver tissue [12]. Furthermore, the viscoelastic properties of a single tissue can vary with age; disease, such as liver fibrosis and multiple sclerosis; and even between malignant and benign tumors [15–18]. In fact, physicians assess the severity of liver fibrosis by measuring the viscoelastic properties with magnetic resonance imaging elastography [19]. In addition to temporal changes of viscoelasticity, spatial heterogeneity can exist within some tissues such as articular cartilage and white matter in the brain [20, 21]. Taken together, the spatiotemporal variations of viscoelasticity within the body may act as a cue to guide specific cellular processes throughout development.

Beyond the documented spatial and temporal heterogeneity of viscoelasticity in tissues, those interested in cell-based therapies may leverage the viscoelasticity of carrier materials to improve the retention, matrix deposition, and therapeutic outcome of cells delivered to a wound site. Consideration of the substrate mechanical properties is especially important in the stem cell community where elasticity alone has been shown to induce and direct the differentiation of hMSCs [5]. Consequently, viscoelastic materials may prove useful for increasing the number and quality of therapeutic cells expanded *in vitro*, which is supported by a recent report showing that hMSC expansion on highly elastic materials (i.e. tissue culture polystyrene) negatively influences the ‘stemness’ of the cells [4]. By more closely recapitulating the mechanical properties of the native tissue microenvironment, viscoelastic biomaterials could enhance the potency of a cellular payload by tailoring the substrate mechanics to elicit a specific cell response. As an example, hMSCs encapsulated in a hydrogel akin to the collagenous phase of bone, which was stiff and rapidly stress relaxing, underwent osteogenic differentiation more efficiently and deposited more mineralized collagen-1 than cells encapsulated in a slower stress relaxing hydrogel [12].

In addition to the aforementioned effects that macroscopic material properties have on cell function, mechanical properties on the micron-scale may play a significant role in mechanotransduction as well. Cells adhere to ECM proteins with focal adhesions that are approximately $0.5\text{--}8\ \mu\text{m}^2$ in size, and consequently, they sense the structure and mechanics of the ECM on a much smaller scale than bulk rheology captures [22, 23]. For example, cells on a substrate with an elasticity gradient will migrate towards the region of greater elasticity by sensing the substrate mechanics with focal adhesions and then, execute a directional decision by evaluating the spatial distribution of stiffness [24]. This process is known as durotaxis, and it provides evidence that micron-scale patterns of mechanical properties, including viscoelasticity, may be a crucial component to the design of materials that promote proper cell function. For this reason, a recent focus has been on the development of methods to fabricate and characterize micron-scale patterns of mechanical properties in soft materials. As a recent example, Ma *et al* leveraged photo-labile hydrogel cross-linkers to create homogeneous and heterogeneous patterns of elasticity with a ‘pixel’ size of $4\ \mu\text{m}^2$ and confirmed the pattern fidelity with atomic force microscopy. It was found that valvular interstitial cells cultured on gels with a heterogeneous pattern of elasticity had smaller focal adhesions, increased rates of proliferation, and decreased markers of myofibroblast activation compared to cells cultured on a homogeneous pattern [25]. Given the physiological relevance of spatially variable biophysical signals on the cell-scale, there exists a need for materials with spatiotemporal control over the viscoelastic properties so that the cellular response to local viscoelasticity can be probed.

Here, we describe the development and characterization of a biocompatible hydrogel capable of photo-induced viscoelasticity. Use of a cross-linker that participates in a radical-mediated addition-fragmentation chain transfer (AFCT) reaction, together with a pendant photoinitiator, enabled hydrogel viscoelasticity during light exposure via cross-link rearrangement. Photo-controlled viscoelasticity was characterized as a function of the light intensity, which is directly related to the photoinitiation rate. The use of a chain transfer agent was also investigated to increase the quantum yield of AFCT and enhance viscoelasticity. Finally, a study was conducted to determine the timescales that cells respond to local sub-cellular changes in the viscoelastic nature of their substrate. The system presented herein provides a user-controlled, dynamic platform to study the role of patterned biophysical signals in mechanotransduction.

2. Materials and methods

All reagents were reagent grade and purchased from commercial sources, unless otherwise noted. $^1\text{H-NMR}$ spectra were collected on a 400 MHz Bruker NMR spectrometer.

Allyl sulfide bis(azide) and azido-RGD (RGD-N₃) were synthesized according to previously described methods [26].

2.1. Synthesis of I2959-NHS

A flame dried 250 ml round bottom flask was charged with anhydrous dimethylformamide (DMF), N,N'-disuccinimidyl carbonate (Sigma, 3.8 g, 15 mmol) and 2-hydroxy-4'-(2-hydroxyethoxy)-2-methylpropiophenone (Irgacure 2959, Ciba, 2.2 g, 10 mmol). The resulting solution was stirred for 5 min while purging with argon. Triethylamine (Sigma, 7.7 ml, 55 mmol) was added dropwise to the reaction vessel with continued purging and then the mixture was stirred overnight at room temperature in the dark. The crude product was concentrated with rotary evaporation to yield dark yellow sap. The crude product was adsorbed onto silica gel and then purified with flash chromatography. The solvent system for chromatography was varied as follows: 1 l of 11:9, 500 ml of 1:1, 500 ml of 2:3, and 500 ml of 0:1 Hexanes:EtOAc. The combined fractions with $R_f = 0.1$ in 11:9 Hexanes:EtOAc were concentrated with rotary evaporation to yield a white powder (1 g, 27% yield). ¹H NMR (400 MHz, Methanol-*d*₄) δ 8.28–8.20 (m, 1 H), 7.07–6.99 (m, 1 H), 4.75–4.68 (m, 1 H), 4.41–4.34 (m, 1 H), 2.84 (s, 2 H), 1.51 (s, 3 H).

2.2. Synthesis of PEG-amine₅-I2959₃

I2959-NHS (55 mg, 98 μ mol, 3/8 eq.) was added to a solution of 8-arm 20 kDa PEG(pentaerythritol)-amine (JenKem Technologies USA, 0.65 g, 260 μ mol amine) and N,N-Diisopropylethylamine (Sigma, 455 μ l, 2.6 mmol, 10 eq.) in anhydrous DCM. The reaction vessel was purged with argon and the mixture was stirred overnight at room temperature. The reaction mixture was precipitated and washed in cold diethyl ether four times and then vacuum dried. The resulting cake was dissolved in deionized water, and dialyzed (22 mm SnakeSkin dialysis tubing, MWCO = 10 kDa) against deionized water for 72 h in the dark. The solution was then lyophilized to obtain the product (PEG-amine₅-I2959₃, 530 mg, 81% yield) as a fluffy white powder. ¹H NMR revealed that functionalization of the PEG-macromer was approximately 38% (i.e. 3 arms were functionalized with I2959, and 5 arms remained amines) by comparing the area of the PEG methylene peak to the I2959 methyl peak.

2.3. Synthesis of PEG-DBCO₃-I2959₃ (PEG-D/I)

A solution of PEG-amine₅-I2959₃ (530 mg, 160 μ mol amine) and N,N-Diisopropylethylamine (83 μ l, 480 μ mol, 3 eq.) in anhydrous DCM was stirred for ten minutes followed by the addition of DBCO-C6-NHS Ester (Click Chemistry Tools, 140 mg, 320 μ mol, 2 eq). The reaction vessel was purged with argon and the mixture was stirred for three days at room temperature. The reaction mixture was precipitated and washed in cold diethyl ether four times, then vacuum dried. The resulting cake was dissolved in deionized water and dialyzed (22 mm SnakeSkin dialysis tubing, MWCO = 10 kDa) against deionized water for 72 h in the dark. The solution was lyophilized to obtain the product (PEG-DBCO₃-I2959₃, 480 mg, 91% yield) as a light-yellow fluffy powder. ¹H NMR revealed that functionalization of the remaining amine arms was approximately 60% (i.e. 3 arms functionalized with DBCO) by comparing the area of the PEG methylene peak to the aromatic DBCO peaks.

2.4. Rheological characterization

Rheology was performed on a TA Instruments AR G2 stress controlled rheometer equipped with an 8 mm sandblasted parallel plate and a quartz plate accessory to allow for controlled illumination. Allyl sulfide cross-linked SPAAC hydrogels were prepared from stock solutions of 20 wt% PEG-DBCO₃-I2959₃ in dimethylsulfoxide (DMSO), 74 mM RGD-N₃ in PBS, and 120 mM AS2N₃ in DMSO. The prepolymer solution was vortexed for 5 s, placed on the rheometer, and the gap was immediately lowered to 300 μ m. Gelation kinetics were evaluated *in situ* by measuring the storage and loss moduli (G' and G'') at an oscillatory shear strain of 10% and a frequency of 1 rad s⁻¹ (within the linear viscoelastic range). Mineral oil was added to the gap to prevent dehydration. The gels were cured for 15 min, after which, the normal force was zeroed and held at 1 N.

2.4.1. Characterization of dynamic moduli

For time-sweep characterization, hydrogels were fabricated on the rheometer by mixing stock solutions to a final concentration of 12 wt% PEG-DBCO₃-I2959₃, 1 mM RGD, and 9.7 mM AS2N₃ in DMSO. The G' and G'' were measured with the fast-sampling mode at an oscillatory shear strain of 10% and a frequency of 1 rad s⁻¹. One minute after the time-sweep step had commenced, the gels were irradiated for 10 s, followed by three minutes of equilibration, and then another time-sweep step.

2.4.2. Characterization of stress relaxation

For stress relaxation characterization, hydrogels were fabricated on the rheometer by mixing stock solutions to a final concentration of 10 wt% PEG-DBCO₃-I2959₃ and 10 mM AS2N₃ in DMSO. The gels were subjected to 10% strain with a rise time of 0.02 s, and after one minute had elapsed the light was turned on for 10 s. The gels were allowed to equilibrate for 2 min before the strain was reapplied.

2.4.3. Characterization of creep

For creep characterization, hydrogels were fabricated on the rheometer by mixing stock solutions to a final concentration of 12 wt% PEG-DBCO₃-I2959₃, 1 mM RGD, and 9.7 mM AS2N₃ in DMSO. The gels were subjected to 100 Pa stress with a rise time of 0.01 s, and after one minute had elapsed the light was turned on for 10 s. The gels were allowed to equilibrate for 2 min before the stress was reapplied.

2.4.4. Statistical analysis

All statistical comparisons and nonlinear regressions were performed in Prism 6 (GraphPad Software, Inc.). For all rheological experiments, at least three replicates were performed. Model parameters were obtained by performing a nonlinear regression on mean creep and stress relaxation data using equations (1) and (2), respectively, with an ordinary least squares approach. All data presented is the mean \pm the standard deviation.

2.5. Cell culture and imaging

2.5.1. Gel fabrication

Allyl sulfide cross-linked SPAAC hydrogels were prepared with stock solutions of 20 wt% PEG-DBCO₃-I2959₃ in dimethylsulfoxide (DMSO), 74 mM RGD-N₃ in PBS, and 120 mM AS2N₃ in DMSO. PEG-DBCO₃-I2959₃ and RGD-N₃ were pre-reacted for 45 min prior to gel fabrication. AS2N₃ was added to the macromer solution to a final concentration of 12 wt% PEG-D/I, 1 mM RGD-N₃, and 9.7 mM AS2N₃ in DMSO. The precursor solution was vortexed for 5 s and dropped onto a microscope slide treated with Sigmacote (Sigma) and a thiol functionalized glass coverslip was placed on top of the precursor solution. The gels were cured for 15 min, soaked in PBS for an additional 10 min, then carefully removed from the microscope slide with razor. The gels were sterilized in 70% EtOH for 10 min, then washed two times and swollen overnight in sterile PBS.

2.5.2. Cell culture

Human mesenchymal stem cells (hMSC) were obtained from RoosterBio Inc. For all experiments, hMSCs were thawed and passaged at 70%–80% confluence at 37 °C and 5% CO₂, with medium changes every 2–3 d (low glucose DMEM supplemented with 10% FBS, 50 U ml⁻¹ of penicillin and streptomycin).

2.5.3. Transfection

To visualize the f-actin cytoskeleton in live cells, hMSCs at passage six were transfected with the mCherry-LifeAct-7 plasmid, which was a gift from Michael Davidson (Addgene plasmid #54 491). Specifically, 3×10^5 hMSCs were transfected with 10 ng mCherry-LifeAct-7 DNA in a 4D Nucleofector (Lonza) using the FF104 program. Transfected hMSCs were incubated for 10 min at room temperature, then seeded directly onto PEG-D/I gels at 4×10^4 cells cm⁻².

2.5.4. Live cell imaging and analysis

For bulk photo-induced viscoelasticity, hMSCs were grown on gels for 24 h, gently washed with PBS, and transferred to a glass bottom 24-well plate (Cellvis), upside-down, with fresh imaging medium (Gibco FluoroBrite DMEM supplemented with 10% FBS). A rubber gasket was placed on top of the gel to preclude movement. The live cells were imaged on an inverted widefield microscope (Nikon Eclipse Ti-E) equipped with a 10x objective and an environmental chamber maintained at 37 °C and 5% CO₂. For local photo-induced viscoelasticity, transfected hMSCs were grown on gels for 24 h were gently washed with PBS and transferred to a glass bottom dish (MatTek, 14 mm, No. 1.5) with fresh imaging medium. To prevent the gel from moving in the dish, a coverslip (20 \times 20 mm) was placed on top of the gel and excess media was aspirated. Live cells were imaged on a confocal microscope (Zeiss LSM 710) equipped with a 40x objective and an environmental chamber maintained at 37 °C and 5% CO₂. Viscoelasticity was induced during imaging by creating a photobleaching experiment with the 405 nm laser in Zen software (Zeiss). In a user defined region, the gels were exposed to five rounds of 405 nm light exposure with a 1.58 μ s pixel dwell, then an image of the actin cytoskeleton was acquired. This process was repeated for 200 cycles, which resulted in 1.6 ms of photo-induced viscoelasticity in the defined region. Image analysis was performed in FIJI [27]. Protrusion retraction was measured by marking the furthest position of the lamellipodia boundary before and after illumination. Proximity to the viscoelastic region was defined as the shortest distance from the lamellipodia boundary to the illuminated region within the cell body.

The percent reduction of area for each protrusion was calculated by creating a binary mask containing the cell body and lamellipodia at each frame. The mask was divided into four quadrants, each containing a protrusion, and the percent area reduction was calculated according to equation (S1), which is available online at stacks.iop.org/NJP/21/045004/mmedia, where A_i is the area of the i th quadrant and A_0 is the initial area of the whole cell.

3. Results and discussion

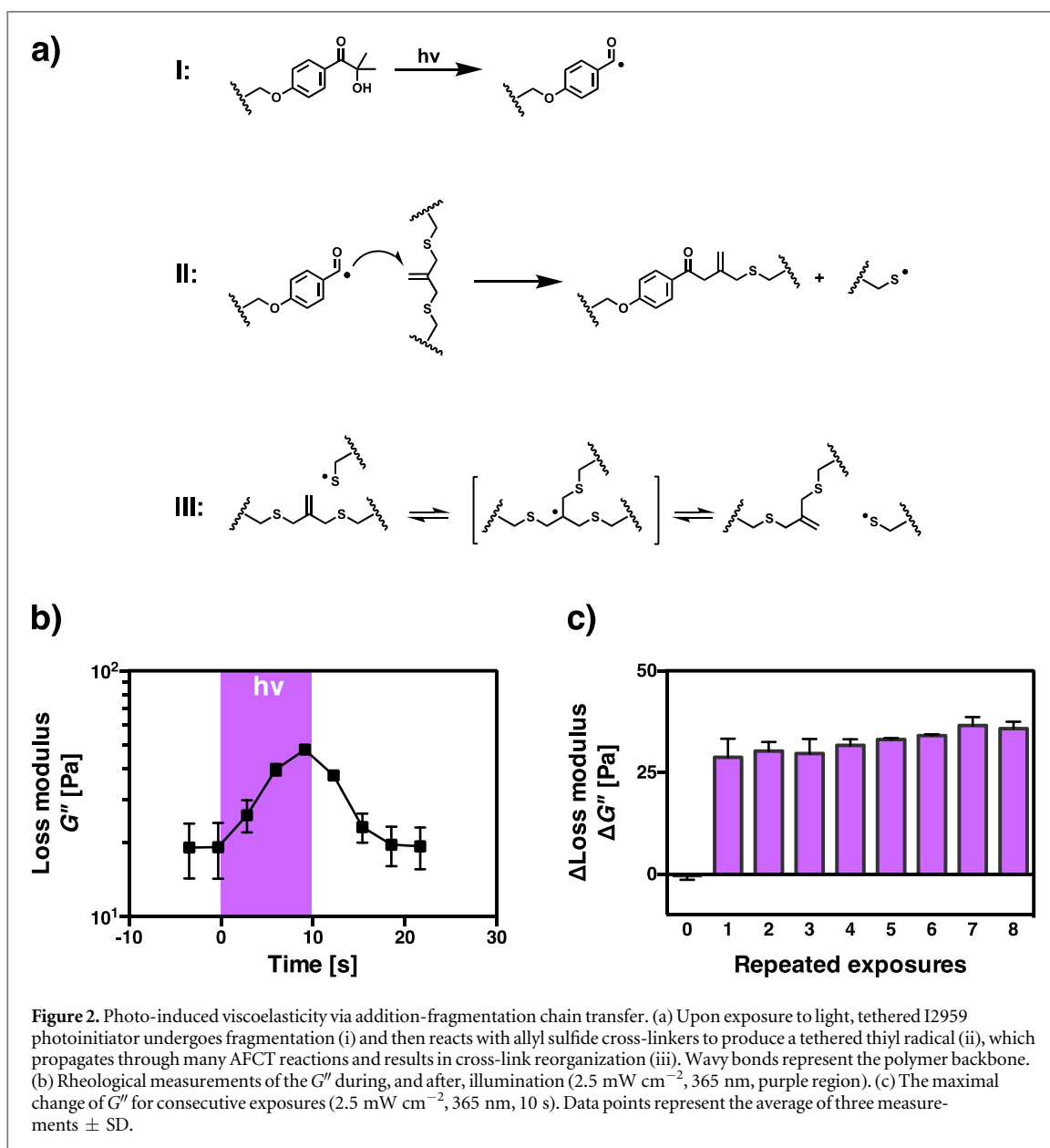
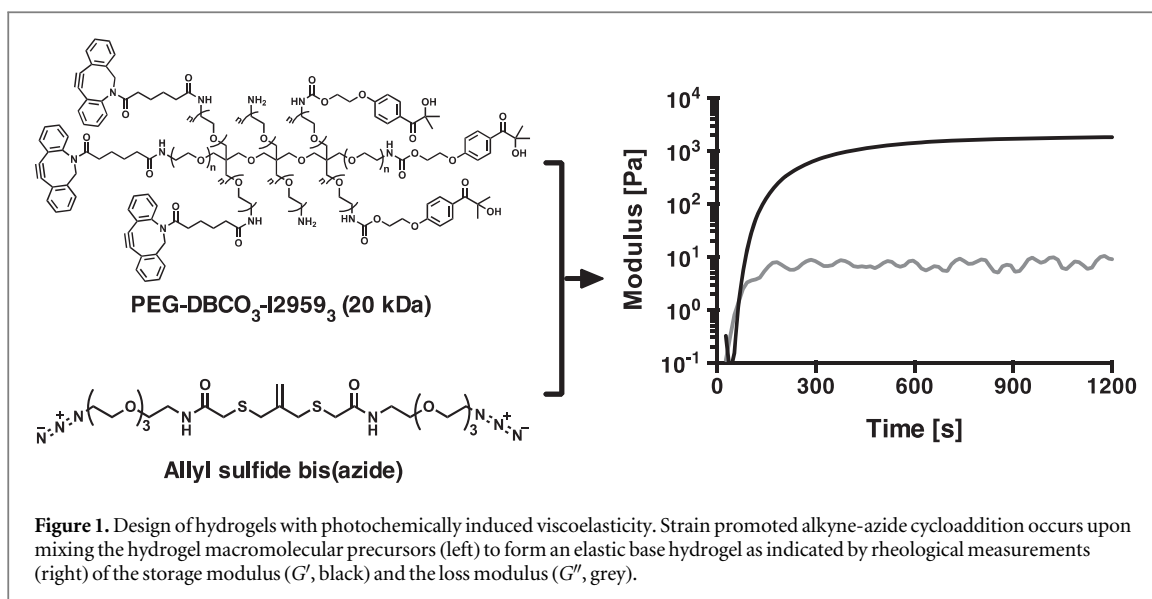
3.1. Design of hydrogels with photochemically derived viscoelasticity

A poly(ethylene glycol) (PEG) based hydrogel was designed with an allyl sulfide cross-linker and a covalently tethered photoinitiator to enable photo-controlled viscoelasticity. There are four advantages of using a network-tethered photoinitiator—as opposed to a soluble photoinitiator—to drive the AFCT process that allows the hydrogel to become viscoelastic. Firstly, a radical derived from a tethered photoinitiator is physically connected to the polymer network, so there is no change in cross-linking from the reaction with an allyl sulfide cross-link. Termination of a network tethered radical with another network radical does, however, result in increased cross-linking. It is also important to note that the tethered photoinitiator is not capable of allyl sulfide cross-link degradation, which has been previously observed with soluble photoinitiators [26]. Secondly, covalent tethering of the photoinitiator to the polymer network prevents cross-link degradation caused by diffusive flux of a soluble photoinitiator from the bulk phase during irradiation. Thirdly, covalent modification of the hydrogel with a photoinitiator eliminates the need to ‘swell’ the photoinitiator into the gel prior to each exposure. Finally, covalent modification of the hydrophobic photoinitiator 2-hydroxy-4’-(2-hydroxyethoxy)-2-methylpropiophenone (I2959) with PEG increases its aqueous solubility, which is reportedly less than 2 wt% [28], allowing one to utilize higher concentrations and achieve longer durations of photoinitiation. I2959 was covalently tethered to the network by use of a multi-armed PEG macromer functionalized with both click-chemistry and photoinitiator groups. I2959 is a Norrish type 1 photoinitiator that absorbs light at 365 nm and 405 nm, making it suitable for initiation on microscope setups [29]. I2959 was selected as the photoinitiator because of its previous use in numerous cell studies with little cytotoxic effects [30, 31]. As an added benefit, I2959 possesses a hydroxy handle, which greatly simplified conjugation to the PEG macromer.

In addition to a tethered photoinitiator, the use of a cross-linker containing the allyl sulfide moiety is key to controlling the viscoelasticity with light. The allyl sulfide moiety is known to participate in a radical-mediated AFCT reaction, which results in covalent adaptability from allyl sulfide rearrangement [32–34]. The adaptable nature of the allyl sulfide cross-linker has previously been leveraged to degrade hydrogels with photo-generated mono-functional thiyl radicals [26]. In this work, however, degradation of the allyl sulfide cross-linker is avoided, and adaptability is retained, by omitting mono-functional thiols and by utilizing a tethered photoinitiator. Formation of the hydrogels was achieved by copolymerizing azide-flanked allyl sulfide cross-linkers (AS2N₃) and six-armed, dibenzocyclooctyne₃/I2959₃ functionalized macromers (PEG-D/I, 20 kDa) through a strain promoted alkyne azide cycloaddition (figure 1(a)). Photo-viscoelastic gels were fabricated by combining PEG-D/I (12 wt%), AS2N₃ (9.7 mM), and the azide functionalized cell adhesion motif RGD-N₃ (1 mM) in DMSO. Rheological measurements revealed that network formation reached completion in approximately 15 min at a final shear storage modulus (G') of 2 kPa and loss modulus (G'') of 20 Pa (figure 1(b)). The $\tan \delta (G'/G'')$ of the base network was 1×10^{-2} , which is characteristic of a purely elastic hydrogel.

Upon excitation by light, the tethered photoinitiator dissociates into two radical species; the ketyl radical species is released into solution and it rapidly reacts with water [29], whereas the benzoyl radical species remains tethered to the network and it either reacts with the allyl sulfide cross-linker or it terminates with another radical species (figure 2(a)). For the AFCT process in this system, a tethered radical (i.e. benzoyl or thiyl) reacts with the allyl sulfide moiety to form an unstable tertiary intermediate. Fragmentation of the intermediate regenerates the allyl sulfide moiety and produces either the original tethered radical, or a new tethered thiyl radical (figure 2(a)). Importantly, AFCT events do not change the cross-linking density and primarily result in the reorganization of the cross-linking structure. Each photo-generated benzoyl radical can trigger multiple AFCT reorganization events in the cross-links, and consequently, a large degree of adaptability can be achieved in the network with a relatively small amount of photo-generated benzoyl radicals.

Photo-induced viscoelasticity of the gels was assessed by monitoring the oscillatory shear G' and G'' *in situ* at 1 rad s^{-1} during exposure to 365 nm light for 10 s at 2.5 mW cm^{-2} . The G' increased to 2.2 kPa (10% increase) post-exposure, which was attributed to secondary cross-linking from a combination of radical-mediated DBCO oligomerization [35] and non-geminate recombination of network tethered radicals (figure S1). The G'' increased asymptotically from 20 to 48 Pa (240% increase) over 10 s of illumination, indicating increased viscoelasticity, then reverted back to 20 Pa within 8 s of the light shuttering off (figure 2(b)). These results suggest that photo-generated I2959 radicals led to photo-induced viscoelasticity of the hydrogels, and moreover, the accumulation of radicals increased the AFCT kinetics over time, and consequently, resulted in the transiently



increasing G'' . In the absence of light, however, the network thiyl radicals terminated, which lead to a loss of viscoelasticity. We further examined the evolution of the complex dynamic modulus during prolonged 180 s exposures and observed that similar to short exposures, the G'' changed rapidly within 10 s of light shuttering. However, we also observed that the G'' and $\tan \delta$ varied during illumination, which was presumably due to photoinitiator consumption (figure S2). For this reason, we limited illumination times to 10 s for subsequent experiments. Photo-induced viscoelasticity in these gels was found to be reproducible over eight successive rounds of 10 s irradiation at 2.5 mW cm^{-2} (figure 2(c)). In support of these results, it was determined that for each exposure the consumption of I2959 was less than 0.01%, and accordingly, the rate of photoinitiation remained essentially constant for each exposure (figure S3(a)). These findings imply that the viscoelasticity, which is dependent on the photoinitiation rate, can be photo-induced for up to an hour without needing to replenish the photoinitiator. At higher light intensities, the viscoelasticity is expected increase at the expense of a shorter duration of photo-induced viscoelasticity.

3.2. The loss modulus scales with photoinitiation rate

We next evaluated the ability to tune the viscoelasticity with the photoinitiation rate, which scales linearly with light intensity (I_0) and I2959 concentration according to equation (1) [36].

$$R_i = \frac{\phi \epsilon f \lambda I_0 C_{I2959}}{N_A h c} . \quad (1)$$

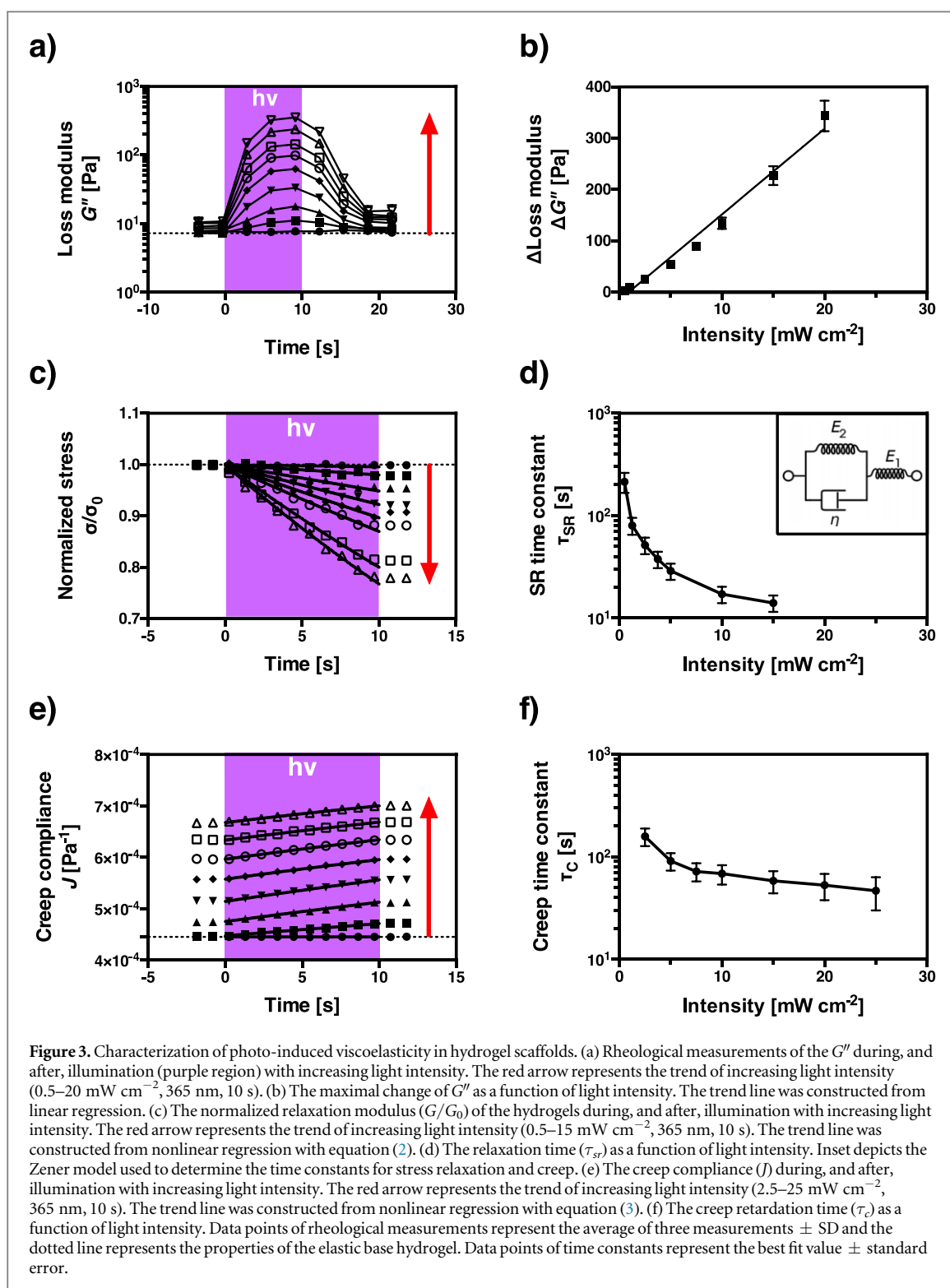
Here, λ is the wavelength of light, ϕ is the quantum yield of photo-fragmentation, ϵ is the molar extinction coefficient of I2959 at λ , and f is the efficiency of photoinitiation (i.e. the probability of benzoyl radicals escaping their nascent solvent cage). I2959 has a reported ϕ of 0.29 and ϵ_{365} of $2.4 \text{ M}^{-1} \text{ cm}^{-1}$ in PBS [29, 37, 38], and for rheological measurements of photo-induced viscoelasticity, a 365 nm light was used at an intensity of $0.5\text{--}25 \text{ mW cm}^{-2}$. For the experimental conditions herein, it was determined that the thin film approximation was valid, and accordingly, the rate of photoinitiation ranged from $0.04\text{--}1.9 \mu\text{M s}^{-1}$ (figure S3(b), (c)). We monitored the G'' *in situ* at 1 rad s^{-1} and 10% strain, while the light source shuttered on for 10 s at $0.5\text{--}20 \text{ mW cm}^{-2}$. We observed that the G'' increased over the illumination period and additionally, the G'' increased more rapidly with increased light intensity (figure 3(a)). Correspondingly, the maximal increase of the G'' increased linearly with the photoinitiation rate (figure 3(b)). It is important to add that hydrogels fabricated without the AFCT cross-linker or the I2959 photoinitiator were found to have a significantly smaller G'' increase compared to hydrogels containing both moieties (figure S4). Together these results support our hypothesis that the hydrogels dissipate stored elastic energy through photoinitiated AFCT cross-link rearrangement and that the rate of AFCT events affects the efficacy of energy dissipation.

3.3. Photo-induced stress relaxation scales with photoinitiation rate

To further verify that photo-induced viscoelasticity was indeed derived from AFCT based network rearrangement—and not an artifact caused by stiffening—stress relaxation was evaluated by measuring the shear stress at 10% strain while the light source shuttered on for 10 s at $0.5\text{--}15 \text{ mW cm}^{-2}$. As expected, we found that the normalized stress (σ/σ_0) decreased as a function of light intensity during light exposure but remained constant in the absence of light. Furthermore, a larger degree of stress relaxation occurred with increasing light intensity (figure 3(c)). In order to calculate the time constant of stress relaxation (τ_{sr}) as a function of light intensity, we fit the shear relaxation modulus (G) to equation (2), which describes stress relaxation in a Zener material.

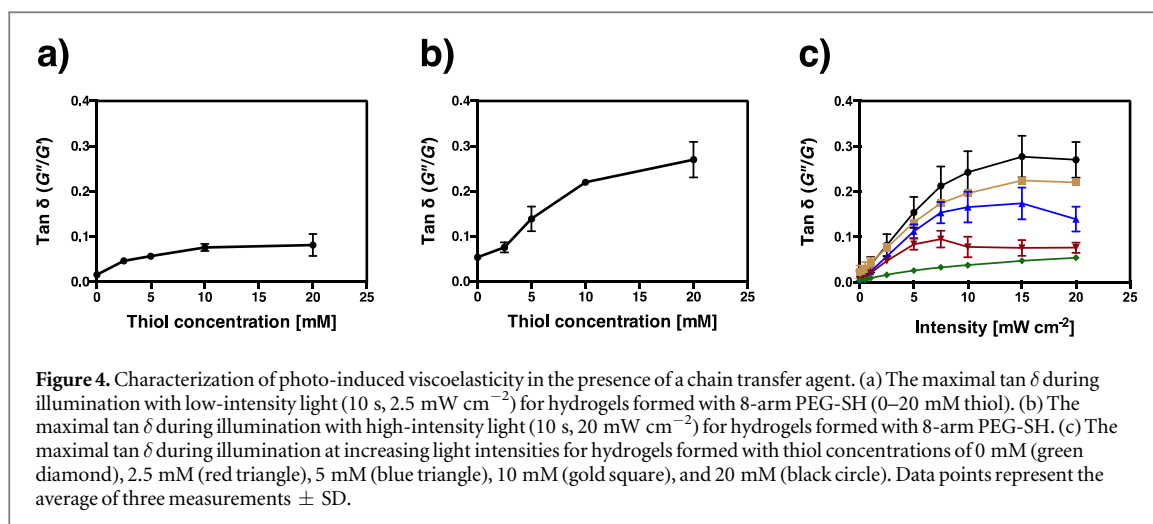
$$G(t) = \frac{\sigma(t)}{\epsilon} = \frac{E_1 E_2}{E_1 + E_2} * \left[1 + \left(\frac{E_1 + E_2}{E_2} - 1 \right) e^{-\frac{t}{\tau_{sr}}} \right] \\ \text{where, } \tau_{sr} = \frac{\eta}{E_1 + E_2} . \quad (2)$$

For equation (2), $\sigma(t)$ represents the shear stress, ϵ represents the applied strain, E_1 and E_2 represent the elastic moduli of the spring elements, and η represents the coefficient of viscosity for the dashpot element (figure 3(d), inset). We found that τ_{sr} decreased from $214 \pm 47 \text{ s}$ to $14.1 \pm 2.6 \text{ s}$ with increased light intensity (figure 3(d)). Again, we ascribed these results to a greater rate of AFCT events with increased photoinitiation rate, and as a result, the gels dissipated the stored elastic energy more rapidly. Unexpectedly, the relationship between τ_{sr} and light intensity was nonlinear, although, this observation might be explained by increased rates of radical termination with higher photoinitiation rates. While the Zener model, which is typically used to describe the viscoelasticity of unreactive systems, successfully illustrated that the rate of stress relaxation scaled with the photoinitiation rate, it is important to note that for this system, η should vary with illumination time because the viscoelastic properties are transient.



3.4. Photo-induced creep scales with photoinitiation rate

Lastly, hydrogel creep was assessed by measuring the shear strain at 100 Pa stress while the light source shuttered on for 10 s at $2.5\text{--}25\text{ mW cm}^{-2}$. As expected, the gels deformed irreversibly during illumination, but did not deform in the absence of light. We also found that the photo-induced creep scaled with light intensity (figure 3(e)). In order to calculate the time constant of creep (τ_c) for each exposure intensity, we fit the creep compliance (J) to equation (3), which describes creep in a Zener material.



$$J(t) = \frac{\epsilon(t)}{\sigma} = \frac{1}{E_1} + \frac{1}{E_2} * (1 - e^{-\frac{t}{\tau_c}})$$

where, $\tau_c = \frac{\eta}{E_2}$. (3)

Similar to stress relaxation, we found that τ_c decreased nonlinearly with increased light intensity, from 158 ± 31 s to 47 ± 17 s (figure 3(f)). Again, we attributed these results to an increased rate of AFCT cross-link rearrangement, which allowed for faster creep. In support of the Zener model, we found that the predicted values of τ_{sr} from the creep test were in good agreement with the measured values of τ_{sr} from the stress relaxation test and differed by a maximum of 32 ± 19 s. Likewise, the predicted values of τ_c from stress relaxation were comparable with the measured values of τ_c from creep and differed by 67 ± 36 s at most. It is also important to point out that, as anticipated, hydrogels fabricated without the AFCT cross-linker or the I2959 photoinitiator did not creep upon light exposure (figure S5). Together, these results reinforce the proposed mechanism of photo-induced viscoelasticity through AFCT based cross-link rearrangement. In accordance with this mechanism, we anticipated that the rate of AFCT events could be further enhanced by limiting benzoyl radical termination through chain transfer pathways.

3.5. Chain transfer enhances photochemically induced viscoelasticity

We next investigated whether multi-functional thiols could boost the rate of AFCT based cross-link rearrangements. We reasoned that free thiols in the system would enhance the rate of AFCT by favoring the rate of benzoyl chain transfer relative to the rate of benzoyl termination. To test this hypothesis, we incorporated 8-arm PEG-thiol (20 kDa, PEG-SH) into our prepolymer formulations at thiol concentrations ranging from 2.5–20 mM. We found that $\tan \delta$ increased asymptotically with thiol concentration, to a value of 0.08 at 2.5 mW cm^{-2} (figure 4(a)) and to a value of 0.27 at 20 mW cm^{-2} (figure 4(b)). Generally, we found that $\tan \delta$ increased with both light intensity and thiol concentration, which confirmed our hypothesis that thiols act to boost the rate of AFCT events (figure 4(c)). With a better understanding of the viscoelastic properties of this photo-controlled system, we were interested in investigating the cellular response to local viscoelasticity changes.

3.6. hMSCs contract in response to bulk and localized photo-induced viscoelasticity

We first cultured hMSCs, which are known to be mechanosensitive [5, 14], on the gels and found that they remained viable and spread by day two. Next, we irradiated the entire gel with 405 nm light at 100 mW cm^{-2} , which results in a photoinitiation rate approximately equivalent to 365 nm light at 0.25 mW cm^{-2} , for 3 min (over 10 min of observation) and noted that the hMSCs contracted and occasionally detached from the substrate. Additionally, we noticed that some cells physically deformed the substrate as they contracted on the viscoelastic substrate (figure S6(a)). Interestingly, we found that the τ_c , which was calculated by tracking the displacement of debris near the cell, was in good agreement with the τ_c estimated from our rheological analysis (figure S6(b), (c)). We further found that hMSCs cultured on glass and elastic hydrogel substrates did not show changes in morphology during exposure—even in the presence of soluble I2959 photoinitiator (figure S7). Collectively, these observations indicate that the photo-induced viscoelasticity of the underlying hydrogel substrate indeed caused the morphological changes observed in the hMSCs.

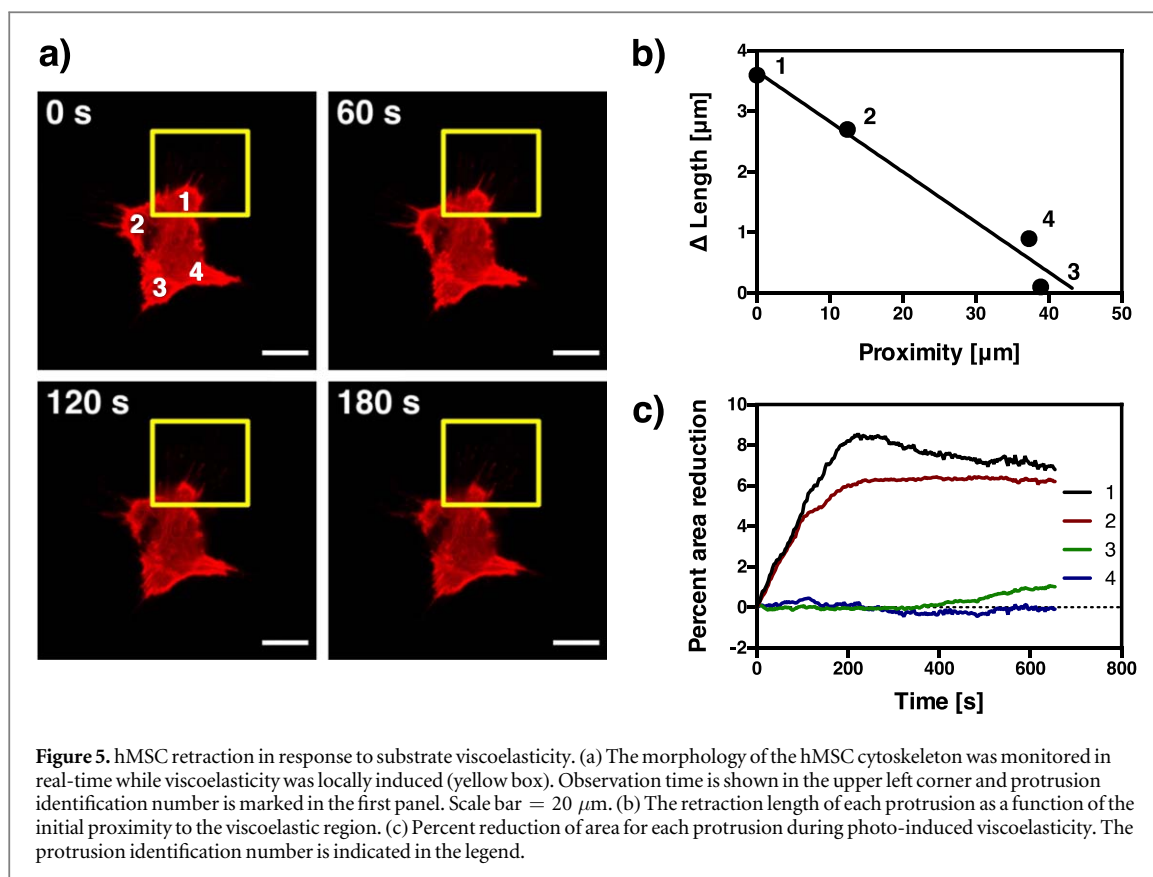


Figure 5. hMSC retraction in response to substrate viscoelasticity. (a) The morphology of the hMSC cytoskeleton was monitored in real-time while viscoelasticity was locally induced (yellow box). Observation time is shown in the upper left corner and protrusion identification number is marked in the first panel. Scale bar = 20 μm. (b) The retraction length of each protrusion as a function of the initial proximity to the viscoelastic region. (c) Percent reduction of area for each protrusion during photo-induced viscoelasticity. The protrusion identification number is indicated in the legend.

Next, in an effort to investigate the effect of localized viscoelasticity on cytoskeletal organization in real-time, we locally induced viscoelasticity under a single cellular protrusion while the other protrusions remained on an elastic substrate. The actin cytoskeleton was visualized in real-time with mCherry-LifeAct over an 11 min period, in which the selected protrusion was illuminated with 405 nm light for 1.6 ms. We observed that all of the protrusions retracted instantaneously in response to the local viscoelasticity change (figure 5(a)). The final retraction length of the protrusions was proportional to the distance from the viscoelastic region, where the protrusion residing on the viscoelastic region had retracted 3.6 μm and a protrusion approximately 37 μm from the viscoelastic region had retracted only 0.9 μm (figure 5(b)). The percent reduction in the area of the protrusions was also proportional to the distance from the viscoelastic region, where the cross-sectional area of the two protrusions closest to the viscoelastic region had decreased over 6% within the first 240 s of exposure (figure 5(c)). At 240 s, the cross-sectional area on the viscoelastic region had decreased by approximately 45%, which could account for the diminished response beyond that time. At 650 s, the total cross-sectional area of the cell had decreased from $1.46 \times 10^3 \mu\text{m}^2$ to $1.25 \times 10^3 \mu\text{m}^2$, representing a 14% reduction in total area. It is difficult to interpret these results in terms of the motor-clutch model because (1) the projected cell area residing on the viscoelastic region decreases over time and (2) the magnitude of viscoelasticity evolves over time, which in turn, alters the period of 'load-and-fail' cycles and thus, the traction force exerted by the cell [39]. However, we ascribed the rapid and far-reaching reduction in the area and length of cellular protrusions upon a local induction of viscoelasticity to the principles of durotaxis and cellular tensegrity [24, 40]. The proposed mechanism for durotaxis predicts that cellular stress relaxation on a viscoelastic gel would decrease the reactive force acting on stress activated channels and stress activated cryptic binding sites, which both affect the local cytoskeletal organization [24]. The tensegrity model of cytoskeletal structure would predict that a local change in actin tension caused by viscoelasticity will affect actin tension in protrusions that are significantly farther from the localized source [40].

The hydrogel materials developed herein are well suited to study the viscoelastic mechanotransduction of cells in real-time. Although the viscoelasticity of these hydrogels is derived from a consumable photoinitiator source, which limits the duration of altered viscoelasticity to minutes or hours, studies on relatively short timescales may still provide valuable insight into mechanotransduction processes that allow cells to quickly sense and respond to the viscoelastic properties of their microenvironment. As an example of short timescale mechanotransduction, Tajik *et al* and Elosegui *et al* recently demonstrated that instantaneous strains applied to focal adhesions increase the diffusivity of transcription factors through the nuclear pore complex and increase mRNA transcription within a minute [41, 42]. The present hydrogel is also unsuitable for cell encapsulation

within a 3D culture context, which is more physiologically relevant than 2D cell culture. 3D culture with these gels is precluded because they are non-degradable, which prohibits cell spreading and causes deleterious effects in certain cell types, including primary hMSCs [43, 44]. In future studies, a cross-linker composed of the allyl sulfide moiety flanked by hydrophilic enzymatically degradable peptide sequences may ameliorate the limited aqueous solubility of the current cross-linker while also allowing for cellularly directed degradation.

4. Conclusion

In this work, a photochemical reaction was leveraged to induce molecular rearrangements on-demand that render the hydrogel networks viscoelastic. The precise location, duration, and magnitude of the hydrogel viscoelasticity was controlled through an AFCT reaction using allyl sulfide cross-linkers and tethered thiyl radicals. Specifically, we demonstrated that $\tan \delta$, creep, and stress relaxation of the hydrogels increase as a function of the photoinitiation rate. Chain transfer via multi-armed PEG thiol was found to further enhance these photo-induced changes in viscoelasticity. As an added benefit, the hydrogels were loaded with large concentrations of a covalently immobilized initiator so that the viscoelasticity changes could be photo-induced at will, without needing to swell photoinitiator into the hydrogel, which can be especially beneficial for studying cellular mechanotransduction. Finally, hMSCs cultured on RGD functionalized allyl sulfide PEG hydrogels spread and were viable throughout the photochemically induced viscoelasticity changes. Upon controlled illumination, hMSCs contracted in response to localized and bulk viscoelasticity changes. The protrusions of hMSCs retracted and decreased in area proportional to their proximity to the local viscoelastic region. While the transient photo-controlled viscoelastic properties of this hydrogel system make it difficult to quantify long-term mechanotransduction in response viscoelasticity, this hydrogel system could be exploited to provide insight into short timescale mechanotransduction processes that allow cells to quickly sense and respond to the viscoelastic properties of their microenvironment as they migrate within it.

Acknowledgments

This work was supported financially in part by grants from the National Science Foundation (DMR 1408955), the National Institutes of Health (R01 DE016523), and the Australian Research Council Discovery Grant (DP140104217). The authors also gratefully acknowledge fellowship support from the NSF GFRP (I.A.M.) and from the Whitaker International Program (I.A.M.). Confocal imaging was performed at the Queensland node of the Australian National Fabrication Facility (ANFF-Q), a company established under the National Collaborative Research Infrastructure Strategy to provide nano- and microfabrication facilities for Australia's researchers. Time-lapse imaging was performed at the BioFrontiers Institute Advanced Light Microscopy Core on a Nikon Ti-E microscope supported by the Howard Hughes Medical Institute. The authors would like to thank Dr Kemal Arda Günay for critically reading the manuscript, as well as Dr Pingping Han for assistance with plasmid production and transfection, and Dr Benoit Maisonneuve for helpful rheological discussions.

References

- [1] Discher D E, Janmey P and Wang Y L 2005 Tissue cells feel and respond to the stiffness of their substrate *Science* **310** 1139–43
- [2] Moore S W, Roca-Cusachs P and Sheetz M P 2010 Stretchy proteins on stretchy substrates: the important elements of integrin-mediated rigidity sensing *Dev. Cell* **19** 194–206
- [3] Wen J H, Vincent L G, Fuhrmann A, Choi Y S, Hribar K C, Taylor-Weiner H, Chen S and Engler A J 2014 Interplay of matrix stiffness and protein tethering in stem cell differentiation *Nat. Mater.* **13** 979–87
- [4] Rao V V, Vu M K, Ma H, Killaars A R and Anseth K S 2019 Rescuing mesenchymal stem cell regenerative properties on hydrogel substrates post serial expansion *Bioeng. Transl. Med.* **4** 51–60
- [5] Engler A J, Sen S, Sweeney H L and Discher D E 2006 Matrix elasticity directs stem cell lineage specification *Cell* **126** 677–89
- [6] Dupont S *et al* 2011 Role of YAP/TAZ in mechanotransduction *Nature* **474** 179–83
- [7] Yang C, Tibbitt M W, Basta L and Anseth K S 2014 Mechanical memory and dosing influence stem cell fate *Nat. Mater.* **13** 645–52
- [8] Alam S G *et al* 2016 The mammalian LINC complex regulates genome transcriptional responses to substrate rigidity *Sci. Rep.* **6** 38063
- [9] Tang S, Ma H, Tu H C, Wang H R, Lin P C and Anseth K S 2018 Adaptable fast relaxing boronate-based hydrogels for probing cell–matrix interactions *Adv. Sci.* **5** 1–8
- [10] Charrier E E, Pogoda K, Wells R G and Janmey P A 2018 Control of cell morphology and differentiation by substrates with independently tunable elasticity and viscous dissipation *Nat. Commun.* **9** 1–13
- [11] Storm C, Pastore J J, MacKintosh F C, Lubensky T C and Janmey P A 2005 Nonlinear elasticity in biological gels *Nature* **435** 191–4
- [12] Chaudhuri O *et al* 2015 Hydrogels with tunable stress relaxation regulate stem cell fate and activity *Nat. Mater.* **15** 326–34
- [13] Cameron A R, Frith J E and Cooper-White J J 2011 The influence of substrate creep on mesenchymal stem cell behaviour and phenotype *Biomaterials* **32** 5979–93
- [14] Cameron A R, Frith J E, Gomez G A, Yap A S and Cooper-White J J 2014 The effect of time-dependent deformation of viscoelastic hydrogels on myogenic induction and Rac1 activity in mesenchymal stem cells *Biomaterials* **35** 1857–68

- [15] Isaksson H, Malkiewicz M, Nowak R, Helminen H J and Jurvelin J S 2010 Rabbit cortical bone tissue increases its elastic stiffness but becomes less viscoelastic with age *Bone* **47** 1030–8
- [16] Salameh N, Peeters F, Sinkus R, Abarca-Quinones J, Annet L, Ter Beek L C, Leclercq I and Van Beers B E 2007 Hepatic viscoelastic parameters measured with MR elastography: correlations with quantitative analysis of liver fibrosis in the rat *J. Magn. Reson. Imaging* **26** 956–62
- [17] Streitberger K J, Sack I, Krefting D, Pfüller C, Braun J, Paul F and Wuerfel J 2012 Brain viscoelasticity alteration in chronic-progressive multiple sclerosis *PLoS One* **7** e29888
- [18] Garteiser P, Doblas S, Daire J L, Wagner M, Leitao H, Vilgrain V, Sinkus R and Van Beers B E 2012 MR elastography of liver tumours: value of viscoelastic properties for tumour characterisation *Eur. Radiol.* **22** 2169–77
- [19] Venkatesh S K, Yin M and Ehman R L 2013 Magnetic resonance elastography of liver: clinical applications *J. Comput. Assist. Tomogr.* **37** 887–96
- [20] Tang S Y, Souza R B, Ries M, Hansma P K, Alliston T and Li X 2011 Local tissue properties of human osteoarthritic cartilage correlate with magnetic resonance T1rho relaxation times *J. Orthop. Res.* **29** 1312–9
- [21] Johnson C L, McGarry M D J, Gharibans A A, Weaver J B, Paulsen K D, Wang H, Olivero W C, Sutton B P and Georgiadis J G 2013 Local mechanical properties of white matter structures in the human brain *Neuroimage* **79** 145–52
- [22] Balaban N Q et al 2001 Force and focal adhesion assembly: a close relationship studied using elastic micropatterned substrates *Nat. Cell Biol.* **3** 466–72
- [23] Fu J, Wang Y K, Yang M T, Desai R A, Yu X, Liu Z and Chen C S 2010 Mechanical regulation of cell function with geometrically modulated elastomeric substrates *Nat. Methods* **7** 733–6
- [24] Lo C-M, Wang H-B, Dembo M and Wang Y-L 2000 Cell movement is guided by the rigidity of the substrate *Biophys. J.* **79** 144–52
- [25] Ma H, Killaars A R, DelRio F W, Yang C and Anseth K S 2017 Myofibroblastic activation of valvular interstitial cells is modulated by spatial variations in matrix elasticity and its organization *Biomaterials* **131** 131–44
- [26] Brown T E, Marozas I A and Anseth K S 2017 Amplified Photodegradation of cell-laden hydrogels via an addition–fragmentation chain transfer reaction *Adv. Mater.* **29** 1605001
- [27] Schindelin J et al 2012 Fiji: an open-source platform for biological-image analysis *Nat. Methods* **9** 676–82
- [28] Fouassier J-P, Burr D and Wieder F 1991 Water-soluble photoinitiators: primary processes in hydroxy alkyl phenyl ketones *J. Polym. Sci. A* **29** 1319–27
- [29] O’Connell C D et al 2018 Tailoring the mechanical properties of gelatin methacryloyl hydrogels through manipulation of the photocrosslinking conditions *Soft Matter* **14** 2142–51
- [30] Bryant S J, Nuttelman C R and Anseth K S 2000 Cytocompatibility of UV and visible light photoinitiating systems on cultured NIH/3T3 fibroblasts *in vitro J. Biomater. Sci. Polym. Ed.* **11** 439–57
- [31] Williams C G, Malik A N, Kim T K, Manson P N and Elisseff J H 2005 Variable cytocompatibility of six cell lines with photoinitiators used for polymerizing hydrogels and cell encapsulation *Biomaterials* **26** 1211–8
- [32] Scott T F, Schneider A D, Cook W D and Bowman C N 2005 Photoinduced plasticity in cross-linked polymers *Science* **308** 1615–7
- [33] Gandavarapu N R, Azagarsamy M A and Anseth K S 2014 Photo-click living strategy for controlled, reversible exchange of biochemical ligands *Adv. Mater.* **26** 2521–6
- [34] Kloxin C J, Scott T F and Bowman C N 2009 Stress relaxation via addition–fragmentation chain transfer in a thiol-ene photopolymerization *Macromolecules* **42** 2551–6
- [35] Brown T E, Silver J S, Worrell B T, Marozas I A, Yavitt F M, Günay K A, Bowman C N and Anseth K S 2018 Secondary photocrosslinking of click hydrogels to probe myoblast mechanotransduction in three dimensions *J. Am. Chem. Soc.* **140** 11585–8
- [36] Odian G 2004 *Principles of Polymerization* (Hoboken, NJ: Wiley)
- [37] Jockusch S, Landis M S, Freiermuth B and Turro N J 2001 Photochemistry and photophysics of α -hydroxy ketones *Macromolecules* **34** 1619–26
- [38] Woodward J R 2002 Radical pairs in solution *Prog. React. Kinet. Mech.* **27** 165–207
- [39] Bangasser B L, Rosenfeld S S and Odde D J 2013 Determinants of maximal force transmission in a motor-clutch model of cell traction in a compliant microenvironment *Biophys. J.* **105** 581–92
- [40] Ingber D E 2003 Tensegrity II. how structural networks influence cellular information processing networks *J. Cell Sci.* **116** 1397–408
- [41] Tajik A, Zhang Y, Wei F, Sun J, Jia Q, Zhou W, Singh R, Khanna N, Belmont A S and Wang N 2016 Transcription upregulation via force-induced direct stretching of chromatin *Nat. Mater.* **15** 1287–96
- [42] Elosgui-Artola A et al 2017 Force triggers YAP nuclear entry by regulating transport across nuclear pores *Cell* **171** 1397–410
- [43] Anderson S B, Lin C-C, Kuntzler D V and Anseth K S 2011 The performance of human mesenchymal stem cells encapsulated in cell-degradable polymer-peptide hydrogels *Biomaterials* **32** 3564–74
- [44] Jongpaiboonkit L, King W J and Murphy W L 2009 Screening for 3D environments that support human mesenchymal stem cell viability using hydrogel arrays *Tissue Eng. A* **15** 343–53